

VASGUIDENET: VASCULAR TOPOLOGY-GUIDED COUINAUD LIVER SEGMENTATION WITH STRUCTURAL CONTRASTIVE LOSS

Chaojie Shen^{1†}, Jingjun Gu^{3†}, Zihao Zhao^{2†}, Ruocheng Li², Cunyuanyang², Jiajun Bu^{2(✉)}, Lei Wu^{2(✉)}

¹ Pujian Medical Technology Co., Ltd., Hangzhou, China

² College of Computer Science and Technology, Zhejiang University, Hangzhou, China

³ Keyi College of Zhejiang Sci-tech University, ShaoXing, China,

qacket@126.com, {gjj, 22221130, lirc, cunyuany, bjj, shenhai1895}@zju.edu.cn,

ABSTRACT

Accurate Couinaud liver segmentation is critical for preoperative surgical planning and tumor localization. However, existing methods primarily rely on image intensity and spatial location cues, without explicitly modeling vascular topology. As a result, they often produce indistinct boundaries near vessels and show limited generalization under anatomical variability. We propose **VasGuideNet**, the first Couinaud segmentation framework explicitly guided by vascular topology. Specifically, skeletonized vessels, Euclidean distance transform (EDT)-derived geometry, and k-nearest neighbor (kNN) connectivity are encoded into topology features using Graph Convolutional Networks (GCNs). These features are then injected into a 3D encoder-decoder backbone via a cross-attention fusion module. To further improve inter-class separability and anatomical consistency, we introduce a **Structural Contrastive Loss (SCL)** with a global memory bank. On Task08_HepaticVessel and our private LASSD dataset, VasGuideNet achieves Dice scores of 83.68% and 76.65% with RVDs of 1.68 and 7.08, respectively. It consistently outperforms representative baselines including UNETR, Swin UNETR, and G-UNETR++, delivering higher Dice/mIoU and lower RVD across datasets, demonstrating its effectiveness for anatomically consistent segmentation. Code is available at <https://github.com/Qacket/VasGuideNet.git>.

Index Terms— Couinaud segmentation, vascular topology, graph convolutional networks (GCNs), structural contrastive loss

1. INTRODUCTION

Couinaud segmentation divides the liver into eight functionally independent segments based on the distribution of the portal and hepatic veins [1, 2]. It provides a critical anatomical basis for surgical planning and postoperative evaluation.

Accurate Couinaud segmentation on preoperative CT is essential for guiding hepatectomy, especially in cases with anatomical variation, as it enables surgeons to determine safe resection boundaries while preserving sufficient functional parenchyma.

Automatic Couinaud segmentation remains highly challenging. Adjacent segments often show similar image intensity and texture patterns, while boundaries near vascular structures are weak or ambiguous. Inter-patient variability, contrast phase differences, and domain shifts across centers further exacerbate these difficulties. Traditional atlas-based and registration methods [3] attempt to impose prior anatomical constraints. However, they struggle with large variations and require extensive preprocessing, which limits clinical applicability.

Recent deep learning methods have significantly advanced liver and Couinaud segmentation. Architectures such as 3D U-Net [4], nnU-Net [5], and Swin UNETR [6] achieve strong single-center results but lose boundary precision near vessels. Transformer-based approaches such as LiverFormer [7] and 3D-HCFormer improve long-range dependency modeling, yet still lack explicit vascular topology encoding.

From the perspective of Couinaud’s anatomical theory, liver segmentation is essentially a functional partitioning process governed by vascular distribution. Previous vascular-related works, such as vesselness filters [8], topology-preserving segmentation [9], and vascular graph representations [10], show the potential of vascular priors, yet they are not explicitly incorporated into Couinaud frameworks.

Moreover, most existing losses such as Dice or Focal primarily optimize voxel-wise accuracy and address class imbalance. However, they do not leverage anatomical priors. This limitation is particularly problematic where inter-segment boundaries are ambiguous near vessels. Contrastive learning [11] has recently been adapted to medical imaging [12, 13] to enforce feature separability and exploit structure, indicating that structural priors can enhance generalization with

[†] Equal contribution;  corresponding author.

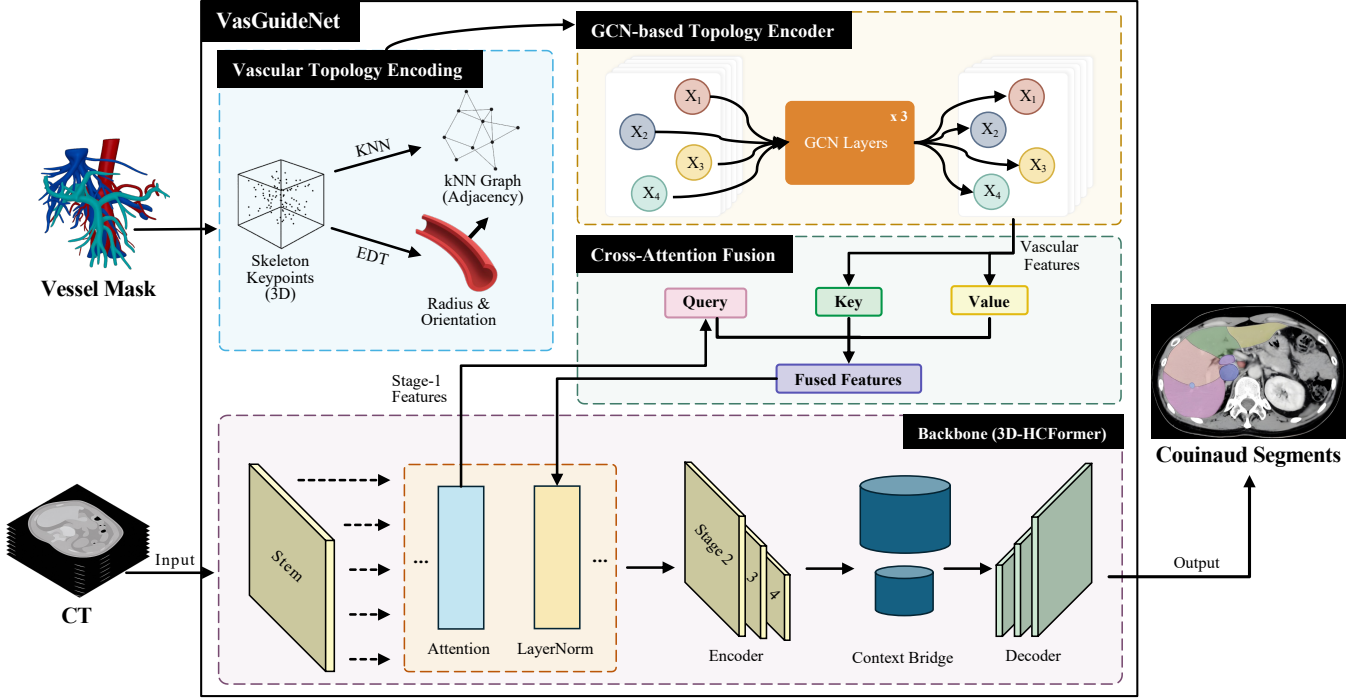


Fig. 1: Overview of VasGuideNet for Couinaud liver segmentation.

limited annotations. These insights motivate the design of a Structural Contrastive Loss (SCL) that leverages vascular guidance for improved robustness under anatomical and acquisition variability.

We study Couinaud segmentation with expert-annotated vessel masks available at both training and inference, focusing on vascular guidance rather than vessel prediction. Based on this setting, we present **VasGuideNet**, a vascular topology-guided Couinaud segmentation framework. The method explicitly encodes vascular skeletons, Euclidean distance transforms, and vessel connectivity graphs. These features are integrated into the segmentation backbone via a GCN-based cross-attention fusion module. Moreover, a Structural Contrastive Loss with a global memory bank is proposed to enforce compact intra-class clusters and well-separated inter-class boundaries. The main contributions of this work are threefold:

- We introduce explicit vascular topology modeling into Couinaud segmentation, enabling boundary refinement near vascular structures.
- We design a GCN-based cross-attention fusion module that integrates topology-aware features with image semantics for anatomically consistent predictions.
- We propose a Structural Contrastive Loss (SCL) with a memory bank to enhance inter-class separability and improve robustness under anatomical and acquisition variability.

2. METHOD

2.1. Network Overview

As shown in Fig. 1, **VasGuideNet** injects vascular topology features into a 3D-HCFormer backbone via cross-attention. The backbone consists of a Stem for downsampling and channel projection, four encoder stages, a Context Bridge for long-range dependencies, and a Decoder. We assume an expert-annotated vessel mask is available at both training and inference; no vessel prediction is used at test time.

2.2. Vascular Topology Encoding

Given a vessel segmentation mask, we first perform 3D skeletonization to obtain the vessel centerline and uniformly sample N skeleton keypoints $\{p_i \in \mathbb{R}^3\}_{i=1}^N$. We then compute the Euclidean distance transform (EDT) of the binary vessel mask. At each keypoint p_i , we extract the local radius $r_i \approx D(p_i)$ and a normalized orientation vector $n_i = \nabla D(p_i) / \|\nabla D(p_i)\|$. Finally, we construct a k -nearest neighbor (kNN) graph over the keypoints to obtain the adjacency matrix A . The initial node feature for each keypoint is computed as

$$h_i^{(0)} = \text{MLP}([p_i, r_i, n_i]), \quad (1)$$

yielding a feature matrix

$$X = [h_i^{(0)}]_{i=1}^N \in \mathbb{R}^{N \times d_0}. \quad (2)$$

2.3. GCN-based Topology Encoder

To capture the connectivity and branching patterns of the hepatic vessel tree, we apply a stack of L graph convolutional layers on the input graph (X, A) :

$$H^{(\ell+1)} = \sigma(\hat{A}H^{(\ell)}W^{(\ell)}), \quad H^{(0)} = X, \quad (3)$$

where \hat{A} is the normalized adjacency matrix with self-loops, $W^{(\ell)}$ are learnable weights, and $\sigma(\cdot)$ denotes a nonlinear activation. The output node embeddings

$$Z = H^{(L)} \in \mathbb{R}^{N \times d} \quad (4)$$

are defined as vascular topology features.

2.4. Vascular Topology Injection

The topology features Z are injected into the backbone via a Transformer-style cross-attention mechanism. Specifically, the Stage-1 encoder output from the backbone is used as Query tokens $Q = FW_Q$, while the topology features provide Key and Value tokens $K = ZW_K$ and $V = ZW_V$. Cross-attention is computed as

$$\text{Attn}(Q, K, V) = \text{softmax}\left(\frac{QK^\top}{\sqrt{d_k}}\right)V, \quad (5)$$

producing fused features that are propagated through the encoder, Context Bridge, and decoder to generate the final prediction.

2.4.1. Ablation fusion variants

For ablation studies, we evaluate three alternative fusion strategies: **No Injection**, which removes the topology branch entirely; **Channel Concatenation**, which concatenates topology and image features before the decoder; and **Distance Bias**, which uses the EDT map as an additive bias to decoder attention weights.

2.5. Loss Function

To enhance inter-class separability and anatomical consistency, we introduce a **Structural Contrastive Loss (SCL)** guided by vascular topology, as illustrated in Fig. 2. SCL selects high-confidence voxels as anchors. These anchors are contrasted against feature centers of other segments, the vessel center, and historical negatives stored in a global memory bank.

2.5.1. Anchor Feature Selection

For each voxel i , let Conf_i denote the predicted confidence. We select anchors above the 95th percentile Q_{95}^{Conf} :

$$A_c = \{F_i \mid \text{Conf}_i > Q_{95}^{\text{Conf}}, M_i = c\}, \quad (6)$$

where F_i is the feature at voxel i , M_i is its ground-truth label, and A_c denotes the anchor set for class c .

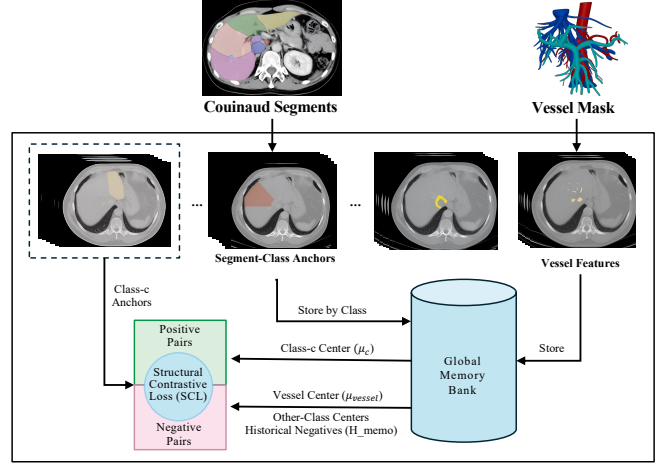


Fig. 2: Structural Contrastive Loss (SCL).

2.5.2. Negative Sample Construction

For each class c , the negative set is defined as

$$B_c = \{\mu_k \mid k \neq c\} \cup \mu_{\text{vessel}} \cup \{H_{\text{memo},k} \mid k \neq c\}, \quad (7)$$

where μ_k is the feature center of class k , μ_{vessel} is the vessel center, and $H_{\text{memo},k}$ denotes historical negatives for class k .

2.5.3. Structural Contrastive Loss

The SCL objective is formulated as

$$\mathcal{L}_{\text{SCL}} = \frac{1}{N} \sum_{c=1}^N \frac{1}{|A_c|} \sum_{a_i \in A_c} -\log \frac{\exp(\text{sim}(a_i, \mu_c)/\tau)}{\sum_{n \in B_c} \exp(\text{sim}(a_i, n)/\tau)}, \quad (8)$$

where $\text{sim}(\cdot, \cdot)$ denotes cosine similarity and τ is a temperature parameter. This objective encourages compact intra-class clusters and well-separated inter-class boundaries.

2.5.4. Memory Bank Update Strategy

We maintain a global memory bank for negative samples and investigate two update strategies: **FIFO**, a first-in-first-out queue that ensures temporal diversity but may discard high-quality entries; and **CATS (Confidence-Aware Time-Slice)**, which preferentially retains high-confidence items and replaces low-confidence ones, improving stability and contrast effectiveness.

3. EXPERIMENTS

We conducted experiments on two liver CT datasets. The first is the **Task08_HepaticVessel** dataset [14] (443 CT scans). Couinaud labels follow prior annotations [15]. The second dataset is the private **LASSD** collection, consisting of 147 CT scans with expert-annotated Couinaud labels provided by our

collaborating hospital. For Task08_HepaticVessel, we use the official vessel annotations for both training and testing; for LASSD, vessel masks are manually annotated by experienced clinical experts and used in the same manner during training and inference.

Segmentation performance is reported in terms of Dice Similarity Coefficient (DSC), mean Intersection over Union (mIoU), and Relative Volume Difference (RVD), which together assess overlap accuracy, boundary precision, and volume consistency.

Table 1: Comparison with state-of-the-art methods (5-fold CV).

Method	DSC (%) \uparrow	mIoU (%) \uparrow	RVD (%) \downarrow
Task08_HepaticVessel			
G-UNETR++	59.32 \pm 2.26	42.78 \pm 2.29	34.11 \pm 3.89
SegMamba	79.05 \pm 3.34	67.61 \pm 3.66	29.34 \pm 15.34
Unetr	81.31 \pm 1.60	57.76 \pm 27.19	27.50 \pm 37.38
LiverFormer	71.51 \pm 1.87	41.60 \pm 19.10	49.24 \pm 31.83
SegFormer	79.51 \pm 1.76	66.79 \pm 2.08	4.80 \pm 0.85
3D-HCFormer	82.23 \pm 0.87	70.61 \pm 1.11	3.50 \pm 1.56
VasGuideNet	83.68 \pm 0.82	72.67 \pm 1.06	1.68 \pm 0.29
LASSD			
G-UNETR++	65.14 \pm 1.55	50.15 \pm 1.49	30.49 \pm 8.51
SegMamba	69.00 \pm 6.28	55.66 \pm 6.71	46.39 \pm 27.09
Unetr	70.03 \pm 6.11	56.48 \pm 6.34	33.04 \pm 23.21
LiverFormer	57.23 \pm 4.51	41.40 \pm 3.86	63.58 \pm 12.30
SegFormer	73.09 \pm 3.53	59.78 \pm 2.87	11.44 \pm 2.12
3D-HCFormer	75.00 \pm 4.01	62.31 \pm 3.50	11.28 \pm 4.79
VasGuideNet	76.65 \pm 3.33	64.40 \pm 2.89	7.08 \pm 1.55

3.1. Comparison with State-of-the-Art

We compare **VasGuideNet** with representative 3D segmentation baselines, including UNETR [16], SegFormer [17], SegMamba [18], G-UNETR++ [19], LiverFormer [7], and 3D-HCFormer. Table 1 summarizes the results.

On **Task08_HepaticVessel**, VasGuideNet achieves the best Dice (83.68%), mIoU (72.67%), and the lowest RVD (1.68). Compared with 3D-HCFormer, it improves Dice by +1.45, mIoU by +2.06, and reduces RVD by 1.82, indicating more accurate boundaries and better volume calibration. On the private **LASSD** dataset, it also outperforms 3D-HCFormer (76.65% vs. 75.00% Dice, 64.40% vs. 62.31% mIoU, 7.08 vs. 11.28 RVD). These results highlight the advantage of explicit vascular-topology modeling under anatomical variability.

3.2. Ablation Studies

3.2.1. Vascular Topology Injection Strategies

We compare the proposed GCN-cross-attention fusion against three alternatives: *None*, *Channel Concatenation*, and *Distance Bias* (Table 2; definitions in Section 2.4.1). Relative to

Table 2: Comparison of Multi-Source Fusion Strategies.

Fusion Strategy	DSC (%) \uparrow	mIoU (%) \uparrow	RVD (%) \downarrow
None	82.23 \pm 0.87	70.61 \pm 1.11	3.50 \pm 1.56
Channel Concatenation	83.23 \pm 1.05	71.91 \pm 1.25	2.23 \pm 0.44
Distance Bias	82.25 \pm 0.63	70.59 \pm 0.72	2.91 \pm 1.05
VasGuideNet	83.68 \pm 0.82	72.67 \pm 1.06	1.68 \pm 0.29

Table 3: SCL update strategies.

Update Strategy	DSC (%) \uparrow	mIoU (%) \uparrow	RVD (%) \downarrow
None	80.30 \pm 0.92	67.76 \pm 1.06	3.12 \pm 0.56
FIFO	83.09 \pm 0.72	71.76 \pm 0.86	1.98 \pm 0.15
CATS	83.68 \pm 0.82	72.67 \pm 1.06	1.68 \pm 0.29

None, VasGuideNet improves Dice by +1.45, mIoU by +2.06, and reduces RVD by 1.82. Channel Concatenation provides moderate gains but still lags behind VasGuideNet, while Distance Bias slightly lowers RVD with limited improvement in Dice/mIoU. These results confirm that explicit topology modeling via GCN-cross-attention is crucial for anatomical consistency.

3.2.2. Structural Contrastive Loss (SCL)

We compare a baseline without SCL, a *FIFO* strategy, and the proposed *CATS* update strategy (Table 3; see Section 2.5.4). Adding SCL markedly improves performance over *None* by +2.79 Dice, +4.00 mIoU, and reduces RVD by 1.14. The confidence-aware *CATS* further surpasses *FIFO* with +0.59 Dice, +0.91 mIoU, and -0.30 RVD, confirming that prioritizing high-confidence features yields more compact clusters and more accurate volumes.

4. CONCLUSION

We present **VasGuideNet**, which encodes skeleton/EDT/kNN vessel topology via GCN and injects it into 3D-HCFormer by cross-attention with SCL. Experiments on Task08_HepaticVessel and the private LASSD dataset demonstrate consistent improvements in Dice and mIoU, as well as reduced RVD, compared with representative baselines. These results highlight the potential of vascular topology guidance for anatomically consistent segmentation, with direct applicability to preoperative surgical planning.

5. ACKNOWLEDGMENTS

This work was supported by Pujian Medical Technology Co., Ltd., Hangzhou, China.

6. COMPLIANCE WITH ETHICAL STANDARDS

The study on Task08_HepaticVessel was conducted retrospectively using human subject data made available in open access by Medical Segmentation Decathlon. Ethical approval was not required as confirmed by the license attached with the open access data. The study on LASSD was performed in line with the principles of the Declaration of Helsinki. Approval was granted by the Ethics Committee of Zhejiang University (No. 202201059).

7. REFERENCES

- [1] Claude Couinaud, *Le foie: Études anatomiques et chirurgicales*, Masson, Paris, 1957.
- [2] John E. Healey and Peter C. Schroy, "Anatomy of the biliary ducts within the human liver," *Archives of Surgery*, vol. 66, no. 5, pp. 599–616, 1953.
- [3] Marius George Linguraru et al., "Hepatic vessel segmentation using graph cuts and shape priors," in *Proceedings of MICCAI*, 2009, pp. 682–689.
- [4] Özgün Çiçek, Ahmed Abdulkadir, S. S. Lienkamp, Thomas Brox, and Olaf Ronneberger, "3d u-net: Learning dense volumetric segmentation from sparse annotation," in *Proceedings of MICCAI*, 2016, pp. 424–432.
- [5] Fabian Isensee, Paul F. Jaeger, Simon A. A. Kohl, Jens Petersen, and Klaus H. Maier-Hein, "nnu-net: A self-adapting framework for u-net-based biomedical image segmentation," *Nature Methods*, vol. 18, no. 2, pp. 203–211, 2021.
- [6] Ali Hatamizadeh et al., "Swin unetr: Swin transformers for semantic segmentation of brain tumors in mri images," in *MICCAI Workshop on Brain Lesion (BrainLes)*, 2022, pp. 272–284.
- [7] W. Qiu et al., "Liverformer: Transformer-based liver segmentation with registration-guided data augmentation," *Medical Image Analysis*, vol. 88, pp. 102840, 2023.
- [8] Alejandro F. Frangi, Wiro J. Niessen, Koen L. Vincken, and Max A. Viergever, "Multiscale vessel enhancement filtering," in *Proceedings of MICCAI*, 1998, pp. 130–137.
- [9] C. Wang et al., "Topology-preserving deep image segmentation using graph convolutional networks," *Medical Image Analysis*, vol. 64, pp. 101717, 2020.
- [10] H. Chen et al., "Vesselgraph: Graph-based representation for vascular structure segmentation," *Medical Image Analysis*, vol. 72, pp. 102139, 2021.
- [11] Kaiming He, Haoqi Fan, Yuxin Wu, Saining Xie, and Ross Girshick, "Momentum contrast for unsupervised visual representation learning," in *Proceedings of CVPR*, 2020, pp. 9729–9738.
- [12] Krishna Chaitanya, Neerav Karani, Christian F. Baumgartner, Anton Becker, Olivia Donati, and Ender Konukoglu, "Contrastive learning of global and local features for medical image segmentation with limited annotations," in *Proceedings of NeurIPS*, 2020, pp. 12546–12558.
- [13] J. Hu et al., "Leveraging structural priors for contrastive learning in medical image segmentation," in *Proceedings of MICCAI*, 2022, pp. 157–167.
- [14] Michela Antonelli, Annika Reinke, Spyridon Bakas, Keyvan Farahani, Annette Kopp-Schneider, Bennett A Landman, Geert Litjens, Bjoern Menze, Olaf Ronneberger, Ronald M Summers, et al., "The medical segmentation decathlon," *Nature communications*, vol. 13, no. 1, pp. 4128, 2022.
- [15] Jiang Tian, Li Liu, Zhongchao Shi, and Feiyu Xu, "Automatic couinaud segmentation from ct volumes on liver using glc-unet," in *International Workshop on Machine Learning in Medical Imaging*. Springer, 2019, pp. 274–282.
- [16] Ali Hatamizadeh, Yucheng Tang, Vishwesh Nath, Dong Yang, Andriy Myronenko, Bennett Landman, Holger R Roth, and Daguang Xu, "Unetr: Transformers for 3d medical image segmentation," in *Proceedings of the IEEE/CVF winter conference on applications of computer vision*, 2022, pp. 574–584.
- [17] Enze Xie, Wenhai Wang, Zhiding Yu, Anima Anandkumar, Jose M Alvarez, and Ping Luo, "Segformer: Simple and efficient design for semantic segmentation with transformers," *Advances in neural information processing systems*, vol. 34, pp. 12077–12090, 2021.
- [18] Zhaohu Xing, Tian Ye, Yijun Yang, Guang Liu, and Lei Zhu, "Segmamba: Long-range sequential modeling mamba for 3d medical image segmentation," in *International conference on medical image computing and computer-assisted intervention*. Springer, 2024, pp. 578–588.
- [19] Seungyoo Lee, Kyujin Han, Hangyeul Shin, Harin Park, Seunghyon Kim, Jeonghun Kim, Xiaopeng Yang, Jae Do Yang, Hee Chul Yu, and Heecheon You, "G-unetr++: a gradient-enhanced network for accurate and robust liver segmentation from computed tomography images," *Applied Sciences*, vol. 15, no. 2, pp. 837, 2025.